Supramolecular nanosheets assembled from poly(ethylene glycol)-b-poly(N-(2-phenylethyl)glycine) diblock copolymer containing crystallizable hydrophobic polypeptoid: crystallization driven assembly transition from filaments to nanosheets

Yuhan Wei[a], Jiliang Tian[a], Zekun Zhang[a], Chenhui Zhu[b], Jing Sun[a*], Zhibo Li[a*]

[a]Key Laboratory of Biobased Polymer Materials, Shandong Provincial Education Department; College of Polymer Science and Engineering, Qingdao University of Science and Technology, Qingdao, 266042, China

[b]Advanced Light Source, Lawrence Berkeley National Laboratory, Berkeley, California 94720, United States

ABSTRACT:

Supramolecular two-dimensional (2D) nanomaterials from block copolymers have received great interests for their unique structure and properties. Here, we report the formation of ultrathin nanosheets from self-assembly of amphiphilic poly(ethylene glycol)-*b*-poly(N-(2-phenylethyl)glycine) (PEG-*b*-PNPE) diblock copolymers, which contain rigid crystallizable polypeptoid segment. The PEG-*b*-PNPE copolymers were synthesized via ring opening polymerization (ROP). The obtained PEG-*b*-PNPE diblock copolymers can spontaneously form highly ordered structures in PEG selective solvents such as water and methanol. The copolymers with short PNPE

segment can directly form nanosheets in water, and the obtained 2D nanosheets have a uniform thickness of 4~5nm. In contrast, the copolymers with relatively long PNPE segment can only assemble into nanosheets with the assistance of methanol. It is proposed that the crystallization and π-π stacking of PNPE blocks play critical roles in the formation of the nanosheet as suggested by grazing incidence wide-angle X-ray scattering (GIWAXS). During the process of adding water into copolymer methanol solution, the nanosheets were observed to evolve from individual nanofibers, to parallel aligning nanofibers, and eventually to the nanosheet structures verified by TEM and cryo-TEM characterizations. We demonstrated that the pre-assembled filaments behave as a fundamental packing motif to align laterally, and further fuse into platelet-like structures. The assembly structure evolution process was tracked by TEM, AFM and cryo-TEM techniques. The understandings of supramolecular 2D nanosheet formation offer a new opportunity to make hierarchical nanostructures from polypeptoids containing copolymers.

Key words: polypeptoid, nanosheet, nanofiber, hierarchical self-assembly

INTRODUCTION

Supramolecular two-dimensional (2D) nanomaterials attract extensive attentions in recent years for their potential applications in sensor, catalysis, biomineralization and drug delivery.[1-6] Most of the work focused on the strategies to construct 2D nanostructures in a controllable manner.[7] Typically, natural biomolecules fold into complex architectures through hierarchical self-assembly. A variety of highly ordered structures with one dimensional geometry in particular have been constructed by pre-assembled subunits of copolymers in solution.[8] However, laterally extended 2D nanosheets are rarely reported through such stepwise self-assembly process.

Bioinspired peptoid-based oligomers have been previously reported to fold into two-dimensional nanosheets.[9-11] Peptoids are structural isomers of peptides, in which the side chains are attached to the amide nitrogen instead of α-carbon. Such structural variation results in the lack of hydrogen-bonding sites and chirality in the main chains, which allows the control of desired interactions through the introduction of specific side chains. The obtained nanosheets from peptoids are particularly interesting, as they serve as a versatile platform for constructing multifunctional scaffolds for many applications.[12-15] For example, Zuckermann *et. al.*, obtained giant, free-floating nanosheets through mixing two oppositely charged peptoid polymers containing N-(2-phenylethyl)glycine (NPE) residues from aqueous solution.[11] They hypothesized that the lateral expansion and contraction of the air-water interface is the main reason for the production of laterally macroscopic nanosheets.[11] They further modified the hydrophobic NPE monomers to investigate the relationship between the peptoid

structure and their ability to form nanosheets.[16] It was demonstrated that the substitution position on the aromatic ring can influence the conformational flexibility of the peptoids, which varied the lateral packing of the aromatic rings in nanosheet formation. Chen group also reported the crystalline nanosheets formed from peptoid oligomers containing N-[2-(4-chlorophenyl)ethyl]glycines residues in aqueous media.[17] However, all of these peptoids were synthesized by solid-phase approach, which allowed unprecedented control over monomer sequence and chain length but with relatively low yield.

In addition to the solid-phase synthesis method, the ring opening polymerization (ROP) technique is an efficient and versatile strategy to synthesize polypeptoids and block copolypeptoids with different functionality.[18-20] One great advantage of this method is that large quantity can be easily achieved. Up to date, only a few self-assemblies such as sphere, cylinder[19, 20] and vesicle[21] have been reported from polypeptoid materials. For example, Zhang group observed morphological transformation from spherical micelles into micrometer-long cylindrical micelles in amphiphilic cyclic and linear poly(N-methylglycine)-b-poly(N-decylglycine) (PNMG-*b*-PNDG) diblock copolypeptoids, which were synthesized by ROP.[22] They further demonstrated the thermo-reversible gelation behaviors of PNMG-*b*-PNDG fibers.[23] Our group has been working on the study of polypeptoid over these years. [24] Recently, our group prepared pH-responsive 2D nanodisk-like structure from a polypeptoid-based triblock copolymer.[25] We further obtained laterally extended 2D nanosheet of poly(ethylene glycol)-block-poly(N-octylglycine) (PEG-*b*-PNOG) in

ethanol and demonstrated that the fusion of 1D spheres and short rods results in the formation of 2D nanosheets.[26] Morphological transition from 1D rods to 2D lamellae has been reported by Eisenberg in the poly(ethylene oxide)-*block*-polycaprolactone (PEO-*b*-PCL) system induced by crystallization-driven self-assembly (CDSA). [27, 28] Later, Manners achieve the dimensional control from 1D fiber to 2D platelets transition by simply alterations in the length of the solubilizing ancillary ligand in square-planar platinum(II) complexes. [29] Nevertheless, more and more attempts have been devoted to construct 2D self-assembly.

In this study, we developed a new strategy to prepare nanosheets with a thickness of merely 4~5 nm in aqueous solution by incorporating π-π interactions of polymers. We designed and synthesized a series of PEG-*b*-poly(N-(2-phenylethyl)glycine) (PEG-*b*-PNPE) diblock copolymers by ROP method using mPEG-NH_2 as macroinitiator. Similar to the reported nanosheet-forming peptoids prepared by solid-phase methods, the phenyl groups were incorporated into the side chains to offer dual hydrophobicity and π-π stacking interactions. These PEG-*b*-PNPE diblocks can form nanosheets and nanofibers in water depending on the chain length of PNPE segment. With the assistance of methanol, which is less selective solvent than water to PNPE segment, all the PEG-*b*-PNPE diblocks form 4~5 nm thickness nanosheets in methanol/H_2O mixture. It is revealed that the nanosheets form through the fusion of the pre-assembled nanofiber motifs in solution as evidenced by the intermediate state of laterally aligning nanofibers by cryo-TEM characterizations.

EXPERIMENTAL SECTION

Materials and methods. Hexane, tetrahydrofuran (THF) and dichloromethane (DCM) were purified by passing through activated alumina columns prior to use. Phosphorus trichloride and trimethylamine were purchased from Sinopharm Chemical reagent co., Ltd. Phenylethylamine, NMP and glyoxylic acid monohydrate were purchased from Aladdin reagent. mPEG-NH_2 (Mn=2000g/mol) was purchased from JenKem Technology Co, Ltd. and dried under vacuum for 24 hrs before use. All other chemicals were purchased from commercial suppliers and used without further purification unless stated. Reaction temperatures were controlled using an IKA temperature modulator. ^{1}H NMR spectra were recorded on Bruker AV500 FT-NMR spectrometer. Tandem Gel permeation chromatography (GPC) was performed at 50°C using an SSI pump connected to Wyatt Optilab DSP with 0.02 M LiBr in DMF as eluent at a flow rate of 1.0 mL/min. All GPC samples were prepared at concentrations of 5-10 mg/mL. The molecular weight was determined by matrix assisted laser desorption/ionization mass spectrometry (Bruker MALDI TOF/TOF Analyzer Microflex LRF) with 10 mg/mL polypeptoid in THF, 1,8,9-tris(Chydroxyanthracene) dissolved in THF at 20 mg/mL and sodium trifluoroacetate at 5mg/mL.

Synthesis of 2-(phen-2-yn-1-ylamino) acetic acid hydrochloric salt (M1). 40 g Glycoxylic acid (50% water solution), 250 mL dichloromethane, and 13.4 g phenylethylamine, were added to a round bottom flask, stirring at room temperature overnight. The CH_2Cl_2 was then removed by rotary evaporation followed by addition of aqueous HCl (200 mL, 1.0 M). The solution was refluxed at 100°C for 20 hrs. After

removing water by rotary evaporation, the solid was purified by recrystallization in methanol/ethyl ether at -20°C overnight. The solid was obtained by filtration and dried under vacuum (8.65 g, 56% yield). ^{1}H NMR (500 MHz, D_2O) δ 7.20 (m, 5H), 3.63 (d, 2H), 3.20 (m, 2H), 2.87 (t, 2H).

Synthesis of 2-((tert-Butoxycarbonyl)(phen-2-yn-1-yl)-amino)acetic acid (M2). The compound **M1** (8.65 g, 40.1 mmol) was dissolved in distilled water (150 mL), followed by addition of di-tert-butyl dicarbonate (30 g, 137 mmol) and triethylamine (40 mL, 286.6 mmol) at room temperature. After stirring for 24 hrs，the reaction mixture was washed with hexane (3×100 mL). Then, the solution pH was adjusted to 3 using 6 M HCl solution. The solution was then extracted with ethyl acetate (3×100 mL). The organic phase was combined and washed with brine twice, and dried over anhydrous Na_2SO_4. The product was collected by rotary evaporator, and dried under vacuum to give a yield of 36%.^{1}H NMR (500 MHz, DMSO) δ 7.20 (m, 5H), 3.63 (d, 2H), 3.20 (m, 2H), 2.87 (t, 2H),1.33 (d, 9H).

Synthesis of N-phenethyl *N*-carboxyanhydride (NPE-NCA). The compound M2 (4.34 g, 13mmol) was dissolved in anhydrous CH_2Cl_2 (250 mL) in a reaction flask with nitrogen inlet cooled in ice bath. PCl_3 (2.3 mL, 26 mmol) was added dropwise to the solution at 0°C. The reaction mixture was stirred for 3.5 hrs before the solvent was removed under vacuum. Anhydrous CH_2Cl_2 (30 mL) was subsequently added and the mixture was filtered. The filtrate was concentrated to afford a white solid. Further recrystallization was performed from anhydrous THF/hexane in a glovebox and white crystals were obtained (2.4 g, 58% yield). Representative FTIR, H^{1}NMR and

C^{13}NMR spectra of NPE-NCA were displayed in Figure S1 (Supporting Information).^{1}H NMR (500 MHz, DMSO) δ 7.40 – 7.16 (m, 5H), 4.25 (s, 2H), 3.50 (d, 2H), 2.84 (t, 2H).

Synthetic of PEG-*b*-poly(*N*-phenethylglycine) (PEG-*b*-PNPE). Synthetic route of the block copolypeptoid by ROP method has been reported before.[25, 26] In this study, NPE-NCA (0.575g, 2.7mmol) and mPEG-NH_2 (Mn = 2000 g/mol) (1.13g, 0.565 mmol) were dissolved in 15 mL dry NMP in a reaction flask. The polymerization was performed under N_2 atmosphere at 55°C and monitored by FTIR until the characteristic peaks (1850 cm^{-1}, 1790 cm^{-1}) of NPE-NCA disappeared. Sample solutions were precipitated into excess hexane. The product was dried under reduced pressure to yield white solid (60% yield). All the other copolymers were prepared in a similar way according to the designed NCA/mPEG-NH_2 ratio.

Preparation of polymer solution. The polymer was directly dispersed in deionized water or methanol at a concentration of 0.5 mg/mL at ambient temperature and the solution was stirred for 2~3 days. For the self-assembly in methanol/H_2O mixture, deionized water was added into the sample methanol solution slowly until the volume ratio of methanol/water reached 2:1. The rate of water addition was about 0.6 mL/min. Then, the solution mixture was stirred for another 2 days. For comparison, solution with different volume ration of methanol/water (v/v) (1:1 and 1:2) was prepared in a similar way.

Characterizations. DSC studies were conducted using a TA DSC 2920 calorimeter. Powder samples enclosed in the aluminum pans were heated from −40°C to 200°C at

10°C/min for three cycles. TEM experiments were conducted on FEI TECNAI 20. Ten microliters of the polymer solution (0.5 mg/mL) was pipetted onto the carbon-coated copper grid, which was pretreated in plasma cleaner. The grid was blotted to remove any excess solution, and then the samples were stained by 0.5% uranyl acetate. The samples were dried under ambient conditions and prepared for TEM characterizations. For cryo-TEM characterization, the specimens were prepared using a Vitrobot (FEI, Inc.). A 5 μL droplet of the aqueous solution at a concentration of 0.5 mg/mL was deposited on the surface of glow discharged grids with lacey carbon films. The droplet was blotted by filter paper for 2s, followed by 2s draining, and then plunged into liquid ethane to obtain a vitrified thin film. The specimen were then stored in liquid nitrogen until they were transferred to a cryogenic sample holder (Gatan 626) and examined using a FEI TECNAI 20 TEM (200 kV) at about -174°C. AFM studies were conducted using tapping mode AFM under ambient conditions. The samples were prepared by spin-coating drops of the polymer solution (0.5 mg/mL) onto the freshly cleaned silica at a spin speed of 1000rpm, and then the samples were stored under ambient conditions before AFM testing. For grazing incidence wide-angle X-ray scattering (GIWAXS Measurements), the polymer solution (0.5 mg/mL) was deposited on Si wafers, dried and stored under ambient conditions before testing. The measurement was performed at beamline 7.3.3, Advanced Light Source (ALS), Lawrence Berkeley National Lab (LBNL). X-ray energy was 10 keV and operated in top off mode. The scattering intensity was recorded on a 2D Pilatus 1M detector (Dectris) with a pixel size of 172 μm. A silver behenate sample was used as a

standard to calibrate the sample-detector distance and the beam position.

RESULTS AND DISCUSSION

The PEG-*b*-PNPE diblock copolymers were synthesized following reported methods[30, 31] and the synthetic route was demonstrated in Figure S2 (Supporting Information). mPEG-NH_2 (Mn =2000) was used as the macroinitiator for all the samples. A series of diblocks were obtained by varying the monomer/macroinitiator ratio from 5 to 40. The chemical structures of the copolymers were confirmed by ^{1}H NMR spectroscopy shown in Figure S3 (Supporting Information). All peaks of the diblock copolymers are well assigned in the ^{1}H NMR spectra, confirming the expected chemical structures. Table 1 summarizes the molecular weight and dispersity ($Đ$) of four samples. The compositions of obtained copolymers were determined by ^{1}H NMR spectroscopy. The DPs were obtained from the proton integral ratios of phenyl group from PNPE block to the ethylene group of PEG block. The GPC traces shown in Figure 1 indicate narrow weight distributions with $Đ \leq 1.25$.

Table1. Molecular characteristics of PEG-*b*-PNPE diblock copolymers.

Samples	Feed ratio (NCA/mPEG-NH_2)[a]	m[b]	Mn[c] (kDa)	Mn[d] (kDa)	Mn[e] (kDa)	Dispersity ($Đ$)[d]
PEG_{44}-*b*-$PNPE_4$	5	4	2.7	3.4	2.9	1.06
PEG_{44}-*b*-$PNPE_9$	15	9	3.5	4.1	3.5	1.06
PEG_{44}-*b*-$PNPE_{16}$	30	16	4.6	5.5	4.2	1.03
PEG_{44}-*b*-$PNPE_{24}$	40	24	5.9	6.9	5.3	1.25

[a]Feed molar ratio of initiator/NPE-NNCA; [b]Calculated from ^{1}H NMR spectra; [c]Calculated from ^{1}H-NMR spectra; [d]Determined from GPC, [e]Determined from MALDI-TOF mass spectrometry..

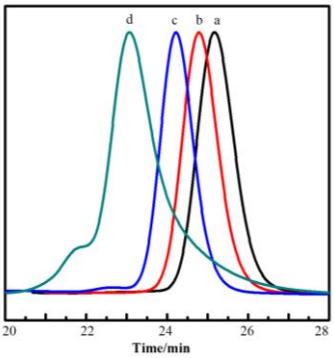

Figure 1. GPC traces of PEG-*b*-PNPE block copolymers: (a) PEG_{44}-*b*-$PNPE_4$; (b) PEG_{44}-*b*-$PNPE_9$; (c) PEG_{44}-*b*-$PNPE_{16}$; (d) PEG_{44}-*b*-$PNPE_{24}$.

The thermal properties of PEG-*b*-PNPE were firstly investigated by DSC characterizations shown in Figure 2. The crystallization temperature (T_c), melting temperature (T_m) and the melting enthalpy (ΔH_m) are summarized in Table S1. Previous studies showed that poly(N-(2-phenylethyl)glycine (PNPE) is crystallizable with a melting transition around ~200°C.[32] In all cases, the DSC endotherms of PEG-*b*-PNPE copolymers display two melting peaks at ~50°C and ~190°C (Figure 2b). Note that the melting transition of PEG homopolymer is at ~53°C (Figure S4). We thus associate the lower melting peak to the melting of PEG crystals while the higher melting peak at 190°C to the melting transition of PNPE domain. In the case of PEG_{44}-*b*-$PNPE_4$ with the shortest PNPE, there is a small peak at 181°C, which indicates that PNPE is partially crystalline. Increasing the DP of the PNPE block promotes the crystallization of the PNPE, as evidenced by the T_m increase from 181°C to 201.2°C with corresponding ΔH_m increase. Accordingly, T_m and ΔH_m of PEG block

decrease correspondingly. Apparently, when the PNPE is very short, the partial crystallization PNPE domains do not affect the crystallization of PEG. However, with increase of PNPE block, crystallization of PNPE block dominates, and the crystallization of PEG is seriously suppressed.[25, 26] DSC cooling curves also shows two crystalline peaks at ~20°C and ~170°C (Figure 2a), which are associated to the crystallization of PEG and PNPE blocks, respectively. With increase of the PNPE chain length, the crystalline temperature of PNPE increases and that of PEG decreases.

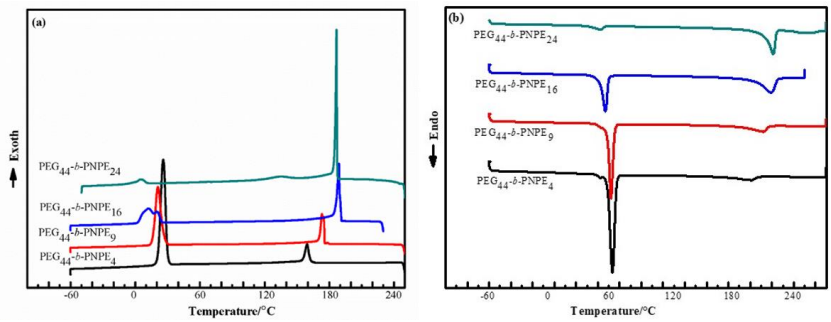

Figure 2. (a) First cooling DSC curves and (b) second heating DSC curves of the four PEG-*b*-PNPE block polymers at 10°C /min.

It is known that PEG dissolves well in water. Initially, it is expected that organic solvent is required as the co-solvent to assist the self-assembling of the PEG-*b*-PNPE copolymers in water due to the crystallization nature of hydrophobic PNPE block. A few different conditions including co-solvent strategy were applied, which was found unnecessary for self-assemblies of all four samples. Possibly, the hydrophobic PNPE

block can interact with water molecules due to the presence of the polar amide bonds, although the interactions are not strong enough to dissolve the PNPE blocks mostly due to the presence of hydrophobic side chains. In contrast, polysarcosine contain one methyl group is soluble in water. Hence, direct dissolution method was applied for the aqueous self-assembly of PEG-*b*-PNPE copolymers at ambient temperature. All four PEG-*b*-PNPE copolymers were directly dispersed in de-ionized water. After stirring for 3 days, the obscure solutions were observed. We then performed TEM characterization to determine the nanostructures. Apparently, PEG_{44}-*b*-$PNPE_4$ diblock with shortest PNPE block spontaneously forms two-dimensional nanosheet-like structures as shown in Figure 3a. Similarly, PEG_{44}-*b*-$PNPE_9$ also self-assembles into nanosheet-like structures (Figure 3b). These 2D nanosheets are about hundreds of nanometers in length for both PEG_{44}-*b*-$PNPE_4$ and PEG_{44}-*b*-$PNPE_9$ samples. AFM characterization shown in Figure 4 verifies the nanosheet-like structures, in consistent with TEM results. In both cases, the nanosheets have low surface roughness, indicating that the nanosheets are extremely flat and uniform. Furthermore, AFM results show that the thickness of the nanosheet is about 5.3 nm for PEG_{44}-*b*-$PNPE_4$ and 4.0 nm for PEG_{44}-*b*-$PNPE_9$, respectively (Figure 4). Note that the thickness of PEG_{44}-*b*-$PNPE_9$ with longer PNPE block is smaller than that of PEG_{44}-*b*-$PNPE_4$. We will address the reasons later. Considering the chain length of PEG-*b*-PNPE diblock copolymer, we assume that these diblock copolymers form bilayer structure, similar to the lipid bilayer. Note that the spontaneous formation of supramolecular nanosheets from nonionic diblock copolymer in aqueous media in large-scale yield has barely

been reported before.[10, 33] In order to exclude the effects of sample preparation process on the nanosheets, cryo-TEM was applied to characterize the pristine state of nanosheets in solution. Following well-established protocol, the sample solution was vitrified into a suspended film in holey TEM grid. Figure 4a shows a typical cryo-TEM image of PEG_{44}-*b*-$PNPE_4$ diblock. An extended nanosheet structure with a length up to 2 μm is clearly observed. The width is about 200~300 nm. Similarly, PEG_{44}-*b*-$PNPE_9$ with longer hydrophobic chain length also forms sheet-like structures, but both the length and width are much smaller than those of PEG_{44}-*b*-$PNPE_4$ diblock. The nanosheets show a homogeneous grayness contrast, indicative of the flat nanostructure consistent with results from TEM and AFM characterizations. This result demonstrates that the nanosheets are not formed during sample preparation process. The nanosheet-like structures with smaller dimensions are also observed in PEG_{44}-*b*-$PNPE_9$ diblock, shown in Figure 4c. It is noteworthy that the nanosheets are highly stable and persist in solution over several months.

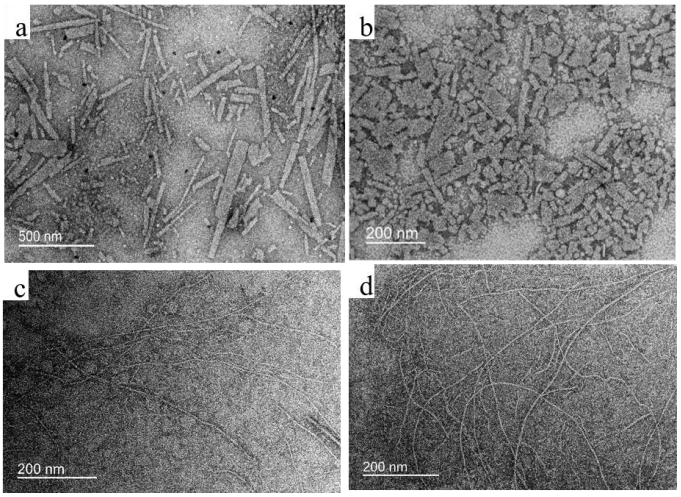

Figure 3. TEM images of the (a): PEG$_{44}$-*b*-PNPE$_4$, (b): PEG$_{44}$-*b*-PNPE$_9$, (c): PEG$_{44}$-*b*-PNPE$_{16}$, (d): PEG$_{44}$-*b*-PNPE$_{24}$, in deionized water.

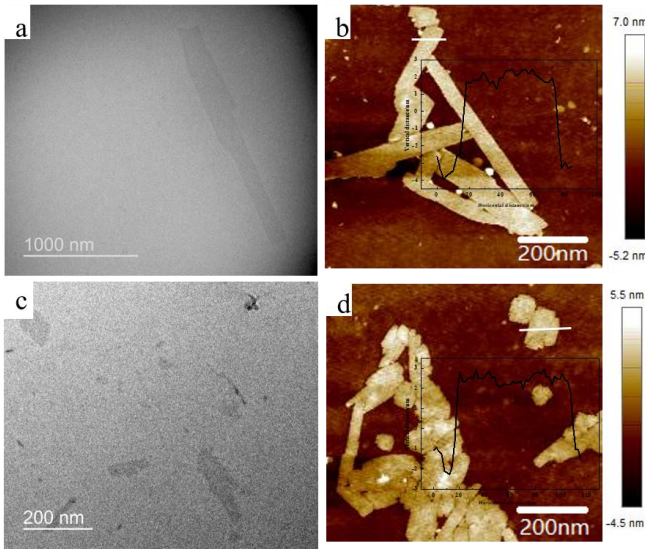

Figure 4. Cryo-TEM images (a, c) and AFM height images (b, d) of PEG-*b*-PNPE

diblock in deionized water. (a, b): PEG_{44}-*b*-$PNPE_4$, (c, d): PEG_{44}-*b*-$PNPE_9$. The inset images of panels b and d are respective height profiles of the areas indicated by the white lines.

Surprisingly, PEG_{44}-*b*-$PNPE_{16}$ and PEG_{44}-*b*-$PNPE_{24}$ copolymers with further increased hydrophobic chain length form nanofibers instead of nanosheets (Figure 3c&3d). Note that the DSC characterization shows that the crystallinity of PNPE block increases substantially with increasing its chain length. This is supposed to facilitate the formation of 2D nanosheet given the stronger crystallization tendency.[26] However, the results are surprisingly opposite to the expectations. We assume such results are caused by the hydrophobic PNPE block with high T_m, which in return will largely limit the chain mobility, similar to an analogue of block copolypeptide system. For example, poly-L-lysine-b-poly-L-leucine (KL) diblock copolypeptides formed hydrogels only as the chain length of poly-L-lysine block was relatively long and poly-L-leucine block has an appropriate chain length.[34, 35] If the poly-L-leucine block is too short, *i.e.*, DP<10, the copolypeptide tends to form micelles. If the poly-L-leucine block is too long, *i.e.*, DP>40, the diblock copolypeptides prefer forming irregular aggregates or precipitation from solution.[36] This is because the reasonable mobility of poly-L-leucine block is prerequisite for the self-assembly of KL diblock. Furthermore, in the case of the diblock copolypeptide with the same chain length and molar composition, varying the hydrophobic poly-L-leucine to other hydrophobic polypeptides such as poly-L-alanine, poly-L-valine, or poly-L-phenylalanine did not guarantee the formation of the hydrogel. The underlying

reason is that both amphiphilic balance and mobility of hydrophobic block are critical for spontaneously self-assembly. The PEG-*b*-polystyrene (PEG-*b*-PS) diblock copolymer is another typical example as well, which has a glassy hydrophobic core. In the absence of co-solvent assistance, PEG-*b*-PS cannot form into supramolecular assemblies spontaneously in water. Here, for the PEG-*b*-PNPE diblock system, we assume that the PNPE block has similar characteristics to that of poly-L-leucine. Firstly, the polar amide group in the backbone of PNPE will offer weak interactions with water molecules. When the PNPE is short, it still has sufficient mobility to adjust its conformation to assemble into ordered hydrophobic domain. The hydrophiphilc PEG block is hydrated to stabilize the supramolecular aggregates. Instead, if the hydrophobic PNPE block is relatively long, it might be trapped and does not have enough mobility to adjust its conformation due to the frozen chains. Hence, it is expected that the nanosheets with short PNPE chain lengths show higher ordering than those in the nanofibers with long chain lengths. Note that the crystallization has been proved to play an important role in the CDSA process. [37] [38, 39] To probe the molecular packing of the nanosheet and nanofiber, grazing incidence wide angle X-ray scattering (GIWAXS) was performed. Figure 5 shows the in-plane line profiles of the nanosheet from PEG_{44}-*b*-$PNPE_4$ and the nanofiber from PEG_{44}-*b*-$PNPE_{24}$, respectively. In both cases, scattering peak at q = 3.83 nm^{-1} is associated to Bragg reflections of PNPE crystals, corresponding to the side chain packing. The spacing is given by $d = 2\pi/q$ = 1.63 nm. In the case of the nanosheet, additional higher-order peak at $3q$ indicates the presence of the lamellae structures. It is assumed that the

spacing of 6Å corresponds to the side-chain dimension of PNPE. The spacing of 4.7Å and 3.9Å are ascribed to the interchain distance and the distance between adjacent monomer residues, respectively. Note that a peak at 4.2Å may indicate the presence of π-π stacking.[40] All these results suggest the nanosheet contains highly crystalline PNPE domains. In the out-of-plane line profile that shown in Figure S5 (Supporting Information), merely broad peaks are shown, confirming the membrane-like nanostructure. In the case of nanofiber, the lack of higher-order peaks and broad peaks in the high *q* range indicates the less ordered packing of the PNPE domains in the nanofibers, shown in both in-plane and out-of-plane line profiles (Figure 5 and Figure S5). Thus, the PNPE block is highly crystalline in nanosheets while less ordered in nanofibers, suggesting that the crystallization of PNPE plays a critical role in the nanosheet formation for direct self-assembly of PEG-*b*-PNPE diblocks in water.

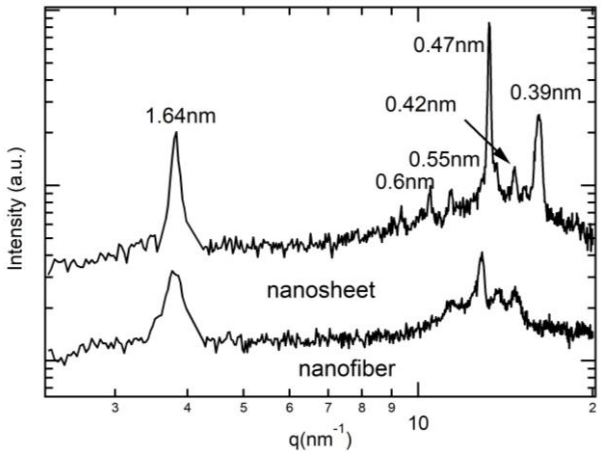

Figure 5. GIWAXS in-plane measurements for assemblies of PEG_{44}-*b*-$PNPE_4$ diblock (top) and PEG_{44}-*b*-$PNPE_{24}$ (bottom).

Due to the hydrated status, the hydrophilic PEG blocks constitute the corona of the aggregates in water. GIWAXS profiles confirm the absence of crystalline PEG domains (Figure 5 and Figure S5), while the PNPE blocks, which are hydrophobic and crystalline, form the innerlayer/core. As the chain length of PNPE is very short (DP = 4), the conformational freedom of the phenyl groups allows for the PNPE chains to adopt optimal packing and crystallization occurs as expected. Note that the flexibility of the polypeptoid backbone lacking hydrogen bonding may also enable the polymer chain to rearrange for the thermodynamically favorable transition. It is likely that the hydrophobic phenyl groups will face up and down in a fully extended conformation in the interior of the nanosheet and the hydrophilic PEG blocks are surface-exposed to construct the nanosheet structure, as shown in Scheme 1. In the case of PEG_{44}-*b*-$PNPE_4$, the extended chain length of PNPE is estimated to be ~1.56 nm by GIWAXS, smaller than the measured thickness of ~5.3 nm by AFM. This is fairly consistent with the proposed structure. Previous report has considered that the polymer solubility is of great significance in the CDSA process. Block copolymers with a shorter core are more soluble, and thus remain as unimers undergoing a slower crystallization process in forming 2D platelets, while copolymers with a longer core are less soluble and thus may form aggregates before crystallization, leading to a less-crystalline 1D cylindrical morphology. [41-43] In this system, the solubility of these four PEG-*b*-PNPE block copolymers in water should be different considering their distinctive block ratios although they are all easily dispersed in water. For PEG_{44}-*b*-$PNPE_4$, it is well soluble and the short PNPE blocks have sufficient mobility

to adjust its conformation and will crystalline slowly to form 2D nanosheet structures with perfect chain folding. With increasing the chain length, the hydrophobicity of the PNPE block in water is increased. In order to minimize the exposure of hydrophobic groups to water, the phenyl group may adopt a less extended geometry. The reduced solubility of PNPE in PEG$_{44}$-*b*-PNPE$_9$ may ~~make the PNPE be trapped in the core partly and have no enough freedom to adjust~~restrict the PNPE to adjust its conformation to form 2D nanosheets with preferred chain-folding. All of these can lead to a reduced sheet thickness (~4.0 nm) in PEG$_{44}$-*b*-PNPE$_9$. While in the cases of both PEG$_{44}$-*b*-PNPE$_{16}$ and PEG$_{44}$-*b*-PNPE$_{24}$ with longer PNPE chain, the hydrophobicity increases and the mobility of PNPE chain can be largely restricted in water as previously proposed. The PNPE has less freedom to adjust its conformation, resulting in less crystalline structure. In this case, the hydrophobic interactions and π-π stacking of PNPE play a critical role in the self-assembly rather than crystallization. Thus, the nanofibers with less ordered structure generate eventually. Generally, semicrystalline block copolymers form self-assemblies with a low curvature of the core-corona interface ~~for the chain folding.~~[44-46] leading to the formation of sheet or lamella. The PEG-*b*-PNPE exhibits the similar behavior in aqueous media.

批注 [z1]: What is this meaning?

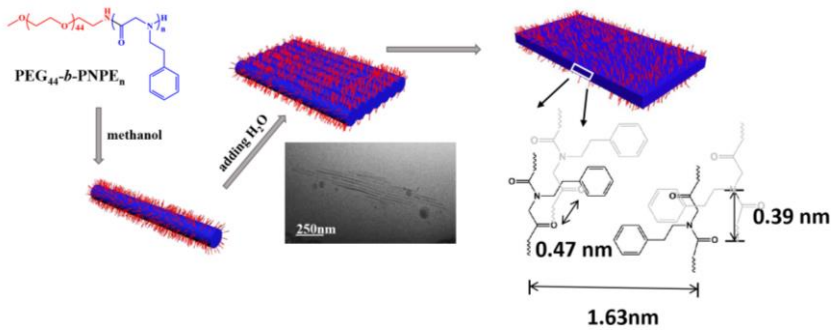

Scheme 1. Possible assembly mechanism of nanosheet for PEG-*b*-PNPE diblocks in selective solvents.

A slow-down self-assembly of PEG-*b*-PNPE diblock ~~would~~ ~~will~~ may expect a structure evolution with time. In order to understand the formation mechanism of the nanosheet, the development of the nanosheet ~~is~~ was tracked in deionized water at different time intervals. A few small aggregates are visible as the aqueous solution is stirred for 40 min, and then nanosheets of tens of nanometers in length appear with increasing stirring time to 60 min (Figure S6). The thickness of the small nanosheet is determined to be 4.0 nm, consistent with those after 3 days stirring (Figure S6b). Increasing stirring time results in the increased population of the nanosheets. After 8 hrs, the cohesion of the nanosheets into large membrane-like structure can be observed. The constant thickness of the nanosheets during the growth process suggests similar molecular packing geometry of the nanosheets with different dimension. Note that the transition from small aggregates to nanosheets in aqueous media is rather fast, so tracing the intermediate state was not successful.

批注 [z2]: 这一段的时态是不是应该为过去时？

If the discussion regarding the self-assembly behaviors of all four PEG_{44}-*b*-$PNPE_m$

copolymers stands, introduction of cosolvent or less selective solvent will facilitate the chain rearrangement of PNPE block and result in formation of more stable nanosheets. Thus, we used methanol with enhanced solubility to PNPE to assist the assembly of copolymers. All of the polypeptoid block copolymers can be readily dispersed in methanol at a concentration of 0.5 mg/mL. One dimensional nanofibers with a length of 100~200nm are exclusively formed for both PEG_{44}-*b*-$PNPE_4$ and PEG_{44}-*b*-$PNPE_9$ (Figure 6) copolymers. Diameters of the nanofibers are about 2.6nm and 1.8nm for PEG_{44}-*b*-$PNPE_4$ and PEG_{44}-*b*-$PNPE_9$ as determined in AFM, respectively. Both are slightly smaller than the thickness of related nanosheets, indicative of the different packing geometry of the polymer chains. The fibers with shorter length are also observed in the solution of PEG_{44}-*b*-$PNPE_{16}$ and PEG_{44}-*b*-$PNPE_{24}$, shown in Figure S7 (Supporting Information). Once formed, these fibers remain unchanged in methanol for several months. Since that methanol is a good solvent for PEG, but selective to PNPE, the PEG-*b*-PNPE block copolymers are thus expected to assemble with PNPE in the core and PEG in the corona. Apparently, the crystallization of PNPE chains is hindered by the presence of methanol. However, we are not able to obtain the detailed nanofiber information by GIWAXS due to the sample-preparation failure because that these fibers prefer to aggregate and fuse to form nanosheet-like structure during drying process (Figure S8).

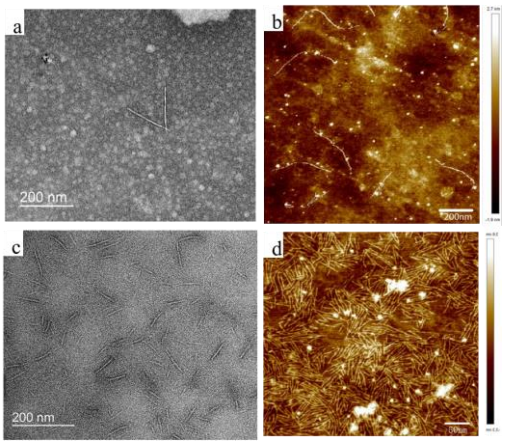

Figure 6. TEM and AFM height images of PEG$_{44}$-*b*-PNPE$_4$ (a, b) and PEG$_{44}$-*b*-PNPE$_9$ (c, d) copolymers in methanol. The sample concentration was 0.5mg/mL.

As deionized water is slowly added into methanol solution of PEG$_{44}$-*b*-PNPE$_4$ at a rate of 0.6 mL/min with varied volume fraction of methanol/H_2O from 2:1 to 1:2, the nanosheets appear in all cases as shown in Figure S9 (Supporting Information). The structural evolution of the self-assembled structure with stirring time after the addition of water is further investigated. Figure 7 display the AFM and TEM images of PEG$_{44}$-*b*-PNPE$_4$ assemblies in 2:1 methanol/H_2O (v/v) at different time intervals. The nanofibers aggregate and array into fringe-like structures with the thickness in the range of 3~4 nm after stirring for 7 hrs, shown in AFM. The thickness is slightly larger than that in methanol, suggesting different packing pattern of the molecules. The TEM image generally shows similar morphology with appearance of a few short rods and irregular nanosheets. Both TEM and AFM show the widths of the nanofiber~~s~~ ~~are~~ is in the range of 6~7 nm (as shown in Figure S10a), twice larger than ~~the~~ its

~~thicknesses~~thickness ~~of the nanofibers~~ (3~4 nm). This may suggest that the obtained nanofibers are most likely nanoribbon-like structure with thinner thickness. Note that the clusters of nanofibers may also fuse into platelet-like structure in the solvent-evaporation process. In order to eliminate the influence during drying process, we performed cryo-TEM to characterize the self-assembled structure of PEG_{44}-*b*-$PNPE_4$ in the solution state (Figure 7b, 7d, 7e). In the cryo-TEM image, it is observed that a cluster of fibers array laterally after stirring for 7 hrs, consistent with those in the dry state. It is thus proposed that the nanosheets could be formed via fusion of adjacent nanofibers through the hydrophobic and π-π stacking interactions of PNEG blocks. Note that such intermediate filament in solution was barely shown in previous studies. Continually stirring the mixed solution to 72 hrs, large nanosheets of hundreds of nanometers in length are observed by cryo-TEM (Figure 7e). In addition, the intermediate status of coexistence of fibers and nanosheets during the transition process is occasionally captured by both cryo-TEM and AFM (Figure 7d, 7f). Small amounts of nanofibers with similar height are adjacent to the nanosheets along the long axis, confirming the formation mechanism of the nanosheet. AFM images show that the thickness of the nanosheet and adjacent arrayed nanofibers are ~5nm, consistent with the nanosheet obtained directly from water. This suggests the identical packing geometry of both cases. Note that the thickness of the self-assemblies increase with the addition of water, ~~both nanosheet and nanofiber is larger than that in methanol~~, which is possibly due to increased dimension upon crystallization.[47]

批注 [z3]: 与哪个比较，厚度增加了。这里不是很清楚。

批注 [z4]: Confusing?

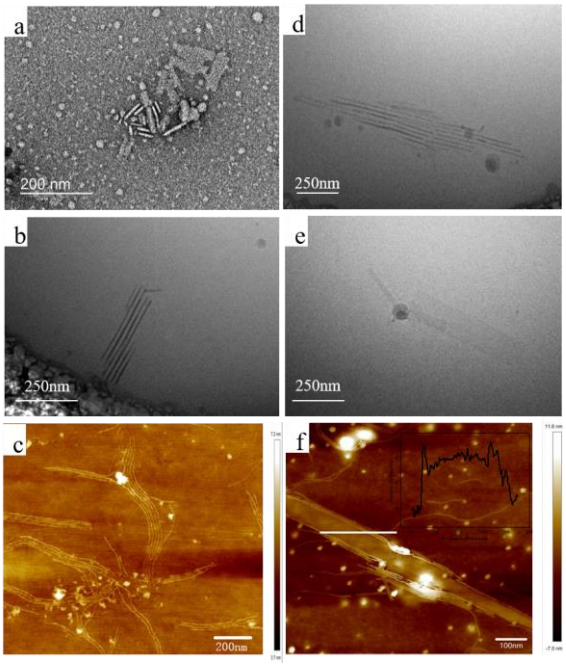

Figure 7. Self-assembled structure of PEG_{44}-*b*-$PNPE_4$ in 2:1 methanol/H_2O (v/v) after stirring at different time intervals: (a, b, c): 7 hrs, (d, e, f): 72 hrs; (a): TEM images; (b, d, e): cryo-TEM; (c, f): respective AFM images.

Evolution of the nanofibers in a series of block copolymers was also investigated. Figure 8 displays the development of the self-assembled structure in PEG_{44}-*b*-$PNPE_9$. Clusters of fibers firstly aggregate and then array laterally along one direction, the nanosheets are barely seen at this moment (Figure 8a, 8b). As increasing the stirring time to 45hrs, nanosheets become the ~~dominant~~ primary assemblies with a few nanofibers adjacent to the edge of the nanosheets, as shown in the AFM image. ~~As~~ When the stirring time increases to 75hrs, a lot of nanosheets are observed along with very few nanofibers. AFM shows quite similar thickness of the nanosheets obtained

from water (4.0 nm) and methanol/H_2O (4.2 nm) solution. Interestingly, the nanosheet-like structure with thicknesses of 5.5 nm and 5.1 nm are also obtained for~~in~~ PEG_{44}-*b*-$PNPE_{16}$ and PEG_{44}-*b*-$PNPE_{24}$ diblocks,~~,~~ respectively~~, as water is added at a rate of 0.6mL/min into their methanol solution~~ (Figure S11). This is possibly due to the enhanced solubility of PNPE in methanol, which facilitates the arrangement of the molecular chains. As the chain length of PNPE increases from 4 to 9, the thickness of the nanosheet decreases. This is possibly due to the less extended structure of the molecular chains, consistent with the previous results of PEG_{44}-*b*-$PNPE_4$ and PEG_{44}-*b*-$PNPE_9$ that directly dispersed in water. Further increasing the chain length of PNPE to 24 results in the increased thickness. In this case, the decreased dimension due to the less extended structure is compromised by the increased chain lengths. ~~The less extended molecular chain results in the small thickness, consistent with the previous results in water.~~

All these results allow us to propose a model for the possible mechanism of the nanofiber-to-nanosheet evolution in methanol/H_2O solution (Scheme1). Note that in the case of water, the PEG-*b*-PNPE diblock copolymer with relative short PNPE block can assemble into highly ordered crystalline nanosheets due to its sufficient mobility to adjust the conformation. In contrast, PEG-*b*-PNPE diblock copolymers with relative long PNPE block lack enough freedom of chain mobility. Accordingly, less ordered nanofibers are preferred instead of more stable nanosheets, consistent with the previously reported structural characteristics of hydrophobic polypeptides. As compared to water, methanol is less selective solvent towards PEG-*b*-PNPE diblock

批注 [z5]: 这个文章里有一个地方不清楚，到底是结晶的 block 厚度大，还是无归排列的 block 厚度大。因为分子量都不是很高，基本算不上聚合物。这个方面的讨论比较混乱。

copolymer. Hence, all four diblock copolymers form nanofiber-like structures with PNPE as the core and PEG as the corona to minimize the exposure of PNPE to the solvent in methanol. Addition of water can increase the solvent selectivity mainly for PNPE block, which results in the formation of more stable nanosheets via rearrangement of hydrophobic domain of the nanofibers. The π-π stacking can further assist the hierarchical evolution from nanofiber to nanosheet, as indicated by GIWAXS results. In addition, due to less solubility in water, the PEG chains may shrink that enable more exposed sticky ends of PNPE blocks to fuse into large nanosheets to avoid energetic penalty.

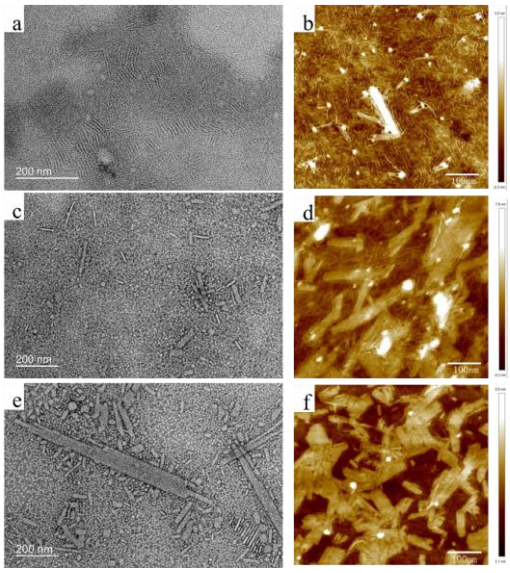

Figure 8. TEM and AFM height images of the self-assembled structure of PEG-*b*-PNPE$_9$ in methanol/H_2O with the ratio 2/1 after stirring for different time: (a, b): 7hrs, (c, d): 45hrs, (e, f): 75hrs.

CONCLUSIONS

In summary, we synthesized a series of polypeptoid-based block copolymers with N-(2-phenylethyl)glycine(Npe) as hydrophobic unit. Two dimensional ultrathin nanosheets of the copolymers with only 4~5nm thickness are easily obtained with shorter PNPE chains in deionized water. GIWAXS results indicate that the dominant driving force of the nanosheet is the crystallization of the PNPE given sufficient mobility. With assistance of methanol, these PEG-*b*-PNPE copolymers with different PNPE chain length entirely form nanosheets in methanol/H_2O mixed solvent. We demonstrated that the PEG-*b*-PNPE first forms the nanofibers in methanol, which serve as fundamental packing motifs to assemble into hierarchical 2D nanosheets by adding water. The intermediate state of laterally aligning filaments in solution is shown by cryo-TEM technique. Both the scalable synthetic method and the excellent biocompatibility make the obtained polypeptoid-based nanosheets potential candidates for the biomedical application.

ASSOCIATED CONTENT

Supporting Information

Additional NMR data, FTIR data, synthetic route, DSC data, GIWAXS result, Fluorescence spectras, TEM image, AFM image.

AUTHOR INFORMATION

Corresponding Authors

*(Z.L.) E-mail zbli@qust.edu.cn; Tel +86 053284022927.

*(J.S.) E-mail jingsun@qust.edu.cn; Tel +86 053284022950.

ACKNOWLEDGMENTS

This work was supported by the National Natural Science Foundation of China (21434008, 21704052, 51722302 and 21674054) and Open Research Fund of State Key Laboratory of Polymer Physics and Chemistry, Changchun Institute of Applied Chemistry, Chinese Academy of Sciences (2017-11). The beamline 7.3.3 at the Advanced Light Source is supported by the Director of the Office of Science, Office of Basic Energy Sciences, of the U.S. Department of Energy under Contract No. DE-AC02-05CH11231.

REFERENCES

1. Boott, C. E.; Nazemi, A.; Manners, I. Synthetic Covalent and Non-Covalent 2D Materials. *Angew. Chem. Int. Ed.* **2015,** *54*, 13876-13894.

2. Cai, S.-L.; Zhang, W.-G.; Zuckermann, R. N.; Li, Z.-T.; Zhao, X.; Liu, Y. The Organic Flatland—Recent Advances in Synthetic 2D Organic Layers. *Adv. Mater.* **2015,** *27*, 5762-5770.

3. Zhuang, X.; Mai, Y.; Wu, D.; Zhang, F.; Feng, X. Two-dimensional soft nanomaterials: a fascinating world of materials. *Adv. Mater.* **2015,** *27*, 403-427.

4. Lin, Y.; Thomas, M. R.; Gelmi, A.; Leonardo, V.; Pashuck, E. T.; Maynard, S. A.; Wang, Y.; Stevens, M. M. Self-Assembled 2D Free-Standing Janus Nanosheets with Single-Layer Thickness. *J.*

Am. Chem. Soc. **2017,** *139*, 13592-13595.

5. Butler, S. Z.; Hollen, S. M.; Cao, L.; Cui, Y.; Gupta, J. A.; Gutiérrez, H. R.; Heinz, T. F.; Hong, S. S.; Huang, J.; Ismach, A. F.; Johnston-Halperin, E.; Kuno, M.; Plashnitsa, V. V.; Robinson, R. D.; Ruoff, R. S.; Salahuddin, S.; Shan, J.; Shi, L.; Spencer, M. G.; Terrones, M.; Windl, W.; Goldberger, J. E. Progress, Challenges, and Opportunities in Two-Dimensional Materials Beyond Graphene. *ACS Nano* **2013,** *7*, 2898-2926.

6. Shah, N. H.; Butterfoss, G. L.; Nguyen, K.; Yoo, B.; Bonneau, R.; Rabenstein, D. L.; Kirshenbaum, K. Oligo(N-aryl glycines): A New Twist on Structured Peptoids. *J. Am. Chem. Soc.* **2008,** *130*, 16622-16632.

7. Colson, J. W.; Dichtel, W. R. Rationally synthesized two-dimensional polymers. *Nat. Chem.* **2013,** *5*, 453-465.

8. Zhang, K.-D.; Tian, J.; Hanifi, D.; Zhang, Y.; Sue, A. C.-H.; Zhou, T.-Y.; Zhang, L.; Zhao, X.; Liu, Y.; Li, Z.-T. Toward a Single-Layer Two-Dimensional Honeycomb Supramolecular Organic Framework in Water. *J. Am. Chem. Soc.* **2013,** *135*, 17913-17918.

9. Hudson, B. C.; Battigelli, A.; Connolly, M. D.; Edison, J.; Spencer, R. K.; Whitelam, S.; Zuckermann, R. N.; Paravastu, A. K. Evidence for cis Amide Bonds in Peptoid Nanosheets. *J. Phys. Chem. Lett.* **2018,** *9*, 2574-2578.

10. Robertson, E. J.; Battigelli, A.; Proulx, C.; Mannige, R. V.; Haxton, T. K.; Yun, L.; Whitelam, S.; Zuckermann, R. N. Design, Synthesis, Assembly, and Engineering of Peptoid Nanosheets. *Acc. Chem. Res.* **2016,** *49*, 379-389.

11. Sanii, B.; Kudirka, R.; Cho, A.; Venkateswaran, N.; Olivier, G. K.; Olson, A. M.; Tran, H.; Harada, R. M.; Tan, L.; Zuckermann, R. N. Shaken, Not Stirred: Collapsing a Peptoid Monolayer To Produce

Free-Floating, Stable Nanosheets. *J. Am. Chem. Soc.* **2011,** *133*, 20808-20815.

12. Sakamoto, J.; van Heijst, J.; Lukin, O.; Schlüter, A. D. Two-Dimensional Polymers: Just a Dream of Synthetic Chemists? *Angew. Chem. Int. Ed.* **2009,** *48*, 1030-1069.

13. Lee, J. H.; Meyer, A. M.; Lim, H.-S. A simple strategy for the construction of combinatorial cyclic peptoid libraries. *Chem. Comm.* **2010,** *46*, 8615-8617.

14. Gangloff, N.; Ulbricht, J.; Lorson, T.; Schlaad, H.; Luxenhofer, R. Peptoids and Polypeptoids at the Frontier of Supra- and Macromolecular Engineering. *Chem. Rev.* **2016,** *116*, 1753-1802.

15. Kudirka, R.; Tran, H.; Sanii, B.; Nam, K. T.; Choi, P. H.; Venkateswaran, N.; Chen, R.; Whitelam, S.; Zuckermann, R. N. Folding of a single-chain, information-rich polypeptoid sequence into a highly ordered nanosheet. *Peptide Science* **2011,** *96*, 586-595.

16. Robertson, E. J.; Proulx, C.; Su, J. K.; Garcia, R. L.; Yoo, S.; Nehls, E. M.; Connolly, M. D.; Taravati, L.; Zuckermann, R. N. Molecular Engineering of the Peptoid Nanosheet Hydrophobic Core. *Langmuir* **2016,** *32*, 11946-11957.

17. Jin, H.; Jiao, F.; Daily, M. D.; Chen, Y.; Yan, F.; Ding, Y.-H.; Zhang, X.; Robertson, E. J.; Baer, M. D.; Chen, C.-L. Highly stable and self-repairing membrane-mimetic 2D nanomaterials assembled from lipid-like peptoids. *Nat. Comm.* **2016,** *7*, 12252.

18. Thielke, M. W.; Secker, C.; Schlaad, H.; Theato, P. Electrospinning of Crystallizable Polypeptoid Fibers. *Macromol Rapid Comm* **2016,** *37*, 100-104.

19. Xuan, S.; Lee, C.-U.; Chen, C.; Doyle, A. B.; Zhang, Y.; Guo, L.; John, V. T.; Hayes, D.; Zhang, D. Thermoreversible and Injectable ABC Polypeptoid Hydrogels: Controlling the Hydrogel Properties through Molecular Design. *Chem. Mater.* **2016,** *28*, 727-737.

20. Li, A.; Zhang, D. Synthesis and Characterization of Cleavable Core-Cross-Linked Micelles Based

on Amphiphilic Block Copolypeptoids as Smart Drug Carriers. *Biomacromolecules* **2016,** *17*, 852-861.

21. Bogomolova, A.; Secker, C.; Koetz, J.; Schlaad, H. Thermo-induced multistep assembly of double-hydrophilic block copolypeptoids in water. *Colloid Polym Sci* **2017,** *295*, 1305-1312.

22. Lee, C.-U.; Smart, T. P.; Guo, L.; Epps, T. H.; Zhang, D. Synthesis and Characterization of Amphiphilic Cyclic Diblock Copolypeptoids from N-Heterocyclic Carbene-Mediated Zwitterionic Polymerization of N-Substituted N-Carboxyanhydride. *Macromolecules* **2011,** *44*, 9574-9585.

23. Lee, C.-U.; Lu, L.; Chen, J.; Garno, J. C.; Zhang, D. Crystallization-Driven Thermoreversible Gelation of Coil-Crystalline Cyclic and Linear Diblock Copolypeptoids. *ACS Macro Lett.* **2013,** *2*, 436-440.

24. Sun, J.; Zhi-bo. Studies on Polypeptoid and Its Structure-Property Relationship. *Acta Polymerica Sinica* **2018**, 1-8.

25. Ni, Y.; Sun, J.; Wei, Y.; Fu, X.; Zhu, C.; Li, Z. Two-Dimensional Supramolecular Assemblies from pH-Responsive Poly(ethyl glycol)-b-poly(l-glutamic acid)-b-poly(N-octylglycine) Triblock Copolymer. *Biomacromolecules* **2017,** *18*, 3367-3374.

26. Shi, Z.; Wei, Y.; Zhu, C.; Sun, J.; Li, Z. Crystallization-Driven Two-Dimensional Nanosheet from Hierarchical Self-Assembly of Polypeptoid-Based Diblock Copolymers. *Macromolecules* **2018,** *51*, 6344-6351.

27. Rizis, G.; van de Ven, T. G. M.; Eisenberg, A. "Raft" Formation by Two-Dimensional Self-Assembly of Block Copolymer Rod Micelles in Aqueous Solution. *Angew. Chem. Int. Ed.* **2014,** *53*, 9000-9003.

28. Rizis, G.; van de Ven, T. G. M.; Eisenberg, A. Homopolymers as Structure-Driving Agents in Semicrystalline Block Copolymer Micelles. *ACS Nano* **2015,** *9*, 3627-3640.

29. Robinson, M. E.; Nazemi, A.; Lunn, D. J.; Hayward, D. W.; Boott, C. E.; Hsiao, M.-S.; Harniman, R. L.; Davis, S. A.; Whittell, G. R.; Richardson, R. M.; De Cola, L.; Manners, I. Dimensional Control and Morphological Transformations of Supramolecular Polymeric Nanofibers Based on Cofacially-Stacked Planar Amphiphilic Platinum(II) Complexes. *ACS Nano* **2017,** *11*, 9162-9175.

30. Lee, C.-U.; Li, A.; Ghale, K.; Zhang, D. Crystallization and Melting Behaviors of Cyclic and Linear Polypeptoids with Alkyl Side Chains. *Macromolecules* **2013,** *46*, 8213-8223.

31. Sun, J.; Černoch, P.; Völkel, A.; Wei, Y.; Ruokolainen, J.; Schlaad, H. Aqueous Self-Assembly of a Protein-Mimetic Ampholytic Block Copolypeptide. *Macromolecules* **2016,** *49*, 5494-5501.

32. Rosales, A. M.; Murnen, H. K.; Zuckermann, R. N.; Segalman, R. A. Control of Crystallization and Melting Behavior in Sequence Specific Polypeptoids. *Macromolecules* **2010,** *43*, 5627-5636.

33. Lin, Y.; Thomas, M. R.; Gelmi, A.; Leonardo, V.; Pashuck, E. T.; Maynard, S. A.; Wang, Y.; Stevens, M. M. Self-Assembled 2D Free-Standing Janus Nanosheets with Single-Layer Thickness. *J. Am. Chem. Soc.* **2017,** *255*, 204-208.

34. Nowak, A. P.; Breedveld, V.; Pakstis, L.; Ozbas, B.; Pine, D. J.; Pochan, D.; Deming, T. J. Rapidly recovering hydrogel scaffolds from self-assembling diblock copolypeptide amphiphiles. *Nature* **2002,** *417*, 424-428.

35. Breedveld, V.; Nowak, A. P.; Sato, J.; Deming, T. J.; Pine, D. J. Rheology of block copolypeptide solutions: Hydrogels with tunable properties. *Macromolecules* **2004,** *37*, 3943-3953.

36. Holowka, E. P.; Pochan, D. J.; Deming, T. J. Charged Polypeptide Vesicles with Controllable Diameter. *J. Am. Chem. Soc.* **2005,** *127*, 12423-12428.

37. Sun, L.; Pitto-Barry, A.; Kirby, N.; Schiller, T. L.; Sanchez, A. M.; Dyson, M. A.; Sloan, J.; Wilson, N. R.; O'Reilly, R. K.; Dove, A. P. Structural reorganization of cylindrical nanoparticles

triggered by polylactide stereocomplexation. *Nat. Comm.* **2014,** *5*, 5746.

38. Wang, Z.; Cao, Y.; Song, J.; Xie, Z.; Wang, Y. Cooperation of Amphiphilicity and Crystallization for Regulating the Self-Assembly of Poly(ethylene glycol)-block-poly(lactic acid) Copolymers. *Langmuir* **2016,** *32*, 9633-9639.

39. Noack, S.; Schanzenbach, D.; Koetz, J.; Schlaad, H. Polylactide-Based Amphiphilic Block Copolymers: Crystallization-Induced Self-Assembly and Stereocomplexation. *Macromol Rapid Comm 0*, 1800639.

40. Chen, C.-L.; Beatty, A. M. Guest Inclusion and Structural Dynamics in 2-D Hydrogen-Bonded Metal−Organic Frameworks. *J. Am. Chem. Soc.* **2008,** *130*, 17222-17223.

41. Yu, W.; Inam, M.; Jones, J. R.; Dove, A. P.; O'Reilly, R. K. Understanding the CDSA of poly(lactide) containing triblock copolymers. *Polym. Chem.* **2017,** *8*, 5504-5512.

42. Inam, M.; Cambridge, G.; Pitto-Barry, A.; Laker, Z. P. L.; Wilson, N. R.; Mathers, R. T.; Dove, A. P.; O'Reilly, R. K. 1D vs. 2D shape selectivity in the crystallization-driven self-assembly of polylactide block copolymers. *Chem. Sci.* **2017,** *8*, 4223-4230.

43. Hsiao, M.-S.; Yusoff, S. F. M.; Winnik, M. A.; Manners, I. Crystallization-Driven Self-Assembly of Block Copolymers with a Short Crystallizable Core-Forming Segment: Controlling Micelle Morphology through the Influence of Molar Mass and Solvent Selectivity. *Macromolecules* **2014,** *47*, 2361-2372.

44. Wei, Y.; Huang, W.; Li, B.; Han, Y.; Pan, C. Square Lamellar Structure Having Phase-Separated Microdomain in H-Shaped Block Copolymer Thin Film. *Macromol Rapid Comm* **2008,** *29*, 1378-1384.

45. Gao, Y.; Qiu, H.; Zhou, H.; Li, X.; Harniman, R.; Winnik, M. A.; Manners, I. Crystallization-Driven Solution Self-Assembly of Block Copolymers with a Photocleavable Junction. *J.*

Am. Chem. Soc. **2015,** *137*, 2203-2206.

46. Gilroy, J. B.; Rupar, P. A.; Whittell, G. R.; Chabanne, L.; Terrill, N. J.; Winnik, M. A.; Manners, I.; Richardson, R. M. Probing the Structure of the Crystalline Core of Field-Aligned, Monodisperse, Cylindrical Polyisoprene-block-Polyferrocenylsilane Micelles in Solution Using Synchrotron Small- and Wide-Angle X-ray Scattering. *J. Am. Chem. Soc.* **2011,** *133*, 17056-17062.

47. Sun, J.; Teran, A. A.; Liao, X.; Balsara, N. P.; Zuckermann, R. N. Crystallization in Sequence-Defined Peptoid Diblock Copolymers Induced by Microphase Separation. *J. Am. Chem. Soc.* **2014,** *136*, 2070-2077.

TOC

Supramolecular nanosheets assembled from poly(ethylene glycol)-b-poly(N-(2-phenylethyl)glycine) diblock copolymer containing crystallizable hydrophobic polypeptoid: crystallization driven assembly transition from filaments to nanosheets

Yuhan Wei[a], Jiliang Tian[a], Zekun Zhang[a], Chenhui Zhu[b], Jing Sun[a*], Zhibo Li[a*]

[a]Key Laboratory of Biobased Polymer Materials, Shandong Provincial Education Department; College of Polymer Science and Engineering, Qingdao University of Science and Technology, Qingdao, 266042, China

[b]Advanced Light Source, Lawrence Berkeley National Laboratory, Berkeley, California 94720, United States